Published in final edited form as:
Acta Biomater. 2010 April ; 6(4): 1640–1648. doi:10.1016/j.actbio.2009.11.011.

Influence of Porosity on Mechanical Properties and *In vivo* Response of Ti6Al4V Implants

Amit Bandyopadhyay[*,1], **Felix Espana**[1], **Vamsi Krishna Balla**[1], **Susmita Bose**[1], **Yusuke Ohgami**[2], and **Neal M Davies**[2]

[1]W. M. Keck Biomedical Materials Research Laboratory, School of Mechanical and Materials Engineering, Washington State University, Pullman, WA 99164-2920, USA

[2]Department of Pharmaceutical Sciences, College of Pharmacy, Washington State University, Pullman, WA 99164-6534, USA

Abstract

Metallic biomaterials are widely used to restore the lost structure and functions of human bone. Due to the large number of joint replacements, there is a growing demand for new and improved orthopedic implants. More specifically, there is a need for novel load bearing metallic implants with low effective modulus matching to that of bone in order to reduce stress shielding and consequent increase in the *in vivo* life-span of the implant. In this study, we have fabricated porous Ti6Al4V alloy structures, using Laser Engineered Net Shaping (LENS™) to demonstrate that advanced manufacturing techniques such as LENS™ can be used to fabricate low-modulus, tailored porosity implants with a wide variety of metals/alloys, where the porosity can be designed in areas based on the patient's need to enhance biological fixation and achieve long-term *in vivo* stability. The effective modulus of Ti6Al4V alloy structures has been tailored between 7 and 60 GPa and porous Ti alloy structures containing 23 to 32 vol. % porosity showed modulus equivalent to human cortical bone. *In vivo* behavior of porous Ti6Al4V alloy samples in male Sprague-Dawley rats for 16 weeks demonstrated significant increase in calcium within the implants indicating excellent biological tissue ingrowth through interconnected porosity. *In vivo* results also showed that total amount of porosity plays an important role in tissue ingrowth.

Keywords

porous Ti6Al4V; *in vivo* behavior; laser engineered net shaping (LENS); mechanical properties

1. Introduction

Currently pure Ti and Ti6Al4V alloys are widely used for load bearing metal implants because of their exceptionally good corrosion resistance and excellent biocompatibility. However, these materials are bioinert and have significantly higher stiffness than natural cortical bone. Although the durability of Ti based total hip replacement (THR) is quite good, some implants still fail as a result of instability and aseptic loosening of the implant, which arises due to: (a) weak interfacial bond between implant surface and living tissue, (b) stress-shielding and (c)

* Corresponding Author's Phone: 1-509-335-4862, Fax: 509-335-4662, amitband@wsu.edu.

wear induced osteolysis. Metallic biomaterials such as Ti develop interfacial fibrous tissue that isolates the implants from their surroundings. Fibrous tissue encapsulation is of concern due to excessive relative micromovement of the device that can occur at the bone–implant interface because of poor interfacial bonding. In addition to this significantly higher elastic modulus of Ti6Al4V alloy implants (114 GPa) than porous natural cortical bone, which is between 10 to 30 GPa, cause the nearby bone to be insufficiently loaded and over time become stress shielded leading to bone resorption and premature failure. This modulus mismatch has been identified as one of the major reasons for stress shielding of bone [1-3]. Furthermore, THR surgeries are being performed with a higher rate of incidence in younger patients, which exposes the implant to greater mechanical stress due to the more active lifestyle of this demographic group over a longer period of time. For these reasons there is a significant demand for improved THR's, and similar load bearing implants, which can perform for a longer lifetime *in vivo*.

In vivo life of load bearing implants can be increased by (i) increasing the interfacial bond between bone tissue and implant materials, and (ii) decreasing the effective modulus of the implants, via compositional or structural modification. The primary function of porosity in orthopedic metal implants is to support tissue adhesion, growth and vascularization. Another desirable property of porous materials for hard tissue repair is the ability to control their elastic modulus to match that of bone, thus reducing the problems associated with stress shielding. Porous materials have been shown to effectively reduce the modulus mismatch and provide stable long-term anchorage for biological fixation of the implant due to bone tissue ingrowth through the pores [4-6]. *In vivo* results of porous Ti implants [7] showed significant increase in osteoconductive properties with increase in total porosity and increasing the pore size increased the amount of new bone growth. Similar influence of porosity on bone ingrowth has also been reported in porous bioactive Ti implants [8].

Conventional powder sintering has been used to fabricate surface treated or fully porous metals for biomedical applications [9-12]. These conventionally sintered metals are often very brittle and are prone to crack propagation at low stresses. Moreover, pore size, shape, volume fraction, and distribution are difficult to control, which have a major influence on mechanical and biological properties. Other fabrication techniques that use foaming agents or molten metal suffer from typical limitations such as contamination, impurity phases, limited and predetermined part geometries, and limited control over the size, shape, and distribution of porosity. Overall, the parts fabricated using the above outlined processes usually suffer from loss of physical properties due to stress concentrations at the porous interface, microstructures changes, and surface contamination from the high temperature sintering process [4,9,10,12, 13-26]. Because of these reasons, fabrication methods for porous metals that can ensure uniform pore size, shape and distribution, and high levels of purity for metals in biomedical applications are in high demand.

Recently advanced laser based solid freeform fabrication (SFF) technologies such as selective laser melting [27] and direct laser sintering [28] have been used to fabricate porous Ti structures. Laser Engineered Net Shaping (LENS™) is one such SFF process that is primarily used to build near net shaped metallic parts. Being a CAD and layer based manufacturing process LENS™ gives a significant advantage over conventional manufacturing methods in terms of controlling the shape, size and internal architecture particularly of porous structures. The schematic representation of the LENS™ process is shown in Figure 1a. Initially, a three-dimensional model of a component to be built is generated using CAD, subsequently a computer program slices the model into a number of horizontal cross-sections or layers. These cross-sections are sequentially created on a substrate producing a three-dimensional object. More detailed description of the process is provided in [5]. Previous work involving LENS™ has been focused on net shape manufacturing [29,30]. Recently this process has also been used

to fabricate net shape porous metals [5,31,32] which have been reported to have superior mechanical, physical, and biological properties.

In this work, we have used LENS™ to fabricate porous samples of Ti6Al4V alloy to enhance biological fixation of the implant via tissue ingrowth though the pores and also to reduce the stiffness mismatches between implants and bone. The objective of our study is to create porous Ti6Al4V alloy structures using LENS™ and to demonstrate that advanced manufacturing techniques such as LENS™ can be used to fabricate tailored porosity implants with variety of metals/alloys, where the porosity can be designed in areas based on the patient's need to enhance biological fixation and achieve long-term *in vivo* stability. LENS™ processed porous Ti6Al4V alloy structures were also evaluated for their *in vivo* performance in male Sprague-Dawley rats up to 16 weeks. Influence of total porosity of LENS™ processed porous Ti6Al4V alloy structures on mechanical properties and *in vivo* performance is discussed in detail.

2. Materials and Methods

2.1 Processing of Porous Ti6Al4V Alloy Structures

Ti6Al4V alloy powder (Advanced Specialty Metals, Inc. NH, USA) with particle size between 45-150 μm was used in this study. The substrates used were rolled commercially pure Ti plates of 3 mm thickness (President Titanium Co., MA, USA). LENS™-750 (Optomec Inc. Albuquerque, NM, USA) with a 500W Nd-YAG laser system was used to fabricate porous Ti6Al4V samples in a glove box with O_2 content less than 10 ppm. Two laser power levels of 180 and 200 W were used to partially melt the alloy powder during the deposition process to create porous structures. In this work, scan speeds of 10, 15, 18, and 25 mm/s and powder feed rates of 15, 20, 30, and 35 g/min were used study their influence on the porosity. Also, in order to control the pore size and distribution, the distance between two titanium alloy tracks was varied between 0.762 and 1.27 mm. Table 1 summarizes different process parameters used in this study.

LENS™ processed parts are produced via layer wise deposition, and each layer consists of a number of consecutive overlapping tracks/scans. The final density of a LENS™ processed part can be considered as the average of the density of each track/scan. Therefore, the extent of powder melting in each track/scan decides the achievable porosity in the final part depending on laser powder (P), scan speed (v), hatch distance or scan line spacing (h) and Z-increment or layer thickness (t). The increase in powder feed rate is reflected in terms of increase in the layer thickness, i.e., layer thickness must be increased to maintain a constant standoff distance between the laser head the substrate. In the present work, all of these parameters are unified into one single factor to understand their influence on the density of LENS™ processed parts. The total energy input per volume of each track/scan (E) as a function of processing parameters was evaluated from [33]:

$$E = \frac{p}{v \cdot h \cdot t} \quad (1)$$

Cylindrical samples with 7 mm and 12 mm diameters were fabricated for compression testing and microstructural evaluation, respectively. Bulk density, which includes both open and closed pores, of the samples was determined by measuring physical dimensions and mass of the samples. Apparent density was measured in water using Archimedes principle. The fraction of open and closed pores in the samples was calculated from the bulk and apparent densities. Microstructures of the samples were examined using both optical and scanning electron microscopes (SEM). Three samples corresponding to each density were compression tested in

a screw driven universal testing machine at a strain rate of 10^{-3} s^{-1}. Polytetrafluoroethylene (PTFE) was used as a lubricant between the sample and compression tools to reduce friction. Young's modulus and 0.2% proof strength were determined from the stress-strain plots derived from load-displacement data recorded during compression testing. For porous elastic materials, the relationship between the elastic modulus and porosity has been widely investigated. In this work an attempt has been made to estimate the Young's modulus of LENS™ processed porous Ti alloy and compared with experimental values using Nielsen's relationship [34]:

$$E = E_m \frac{(1-\nu)^2}{1+\left(\frac{1}{\rho}-1\right)\nu} \quad (2),$$

where: E = Young's modulus of porous material; E_m = Young's modulus of pore free / fully dense material; ν = Volume fraction of porosity; ρ = Geometry factor based on pore shape. (In the present work geometry factor was taken as the roundness of the pores computed as: $\frac{4 \times \pi \times Area}{Perimeter^2}$).

Vicker's microhardness measurements (Leco, M400G3 model) were performed on the laser processed Ti6Al4V alloy samples using 200g load for 15s. An average value of 10 measurements on each sample was reported and compared with conventionally processed Ti6Al4V.

2.2 In vivo Study

2.2.1 Porous Ti6Al4V alloy Implants—LENS™ parameters used to fabricate porous Ti6Al4V alloy samples for *in vivo* study are shown in Table 2. Porous Ti alloy samples with 3 mm diameter and 6 mm in length were used for *in vivo* study. Samples with three different densities, i.e., 75%, 89.3% and 97.2%, were used to study the influence of porosity on biological tissue ingrowth as a function of implantation time up to 16 weeks. Ti alloy sample with 97.2% density was used as control.

2.2.2 Surgical Procedure—Male Sprague-Dawley rats (280-300 grams, Charles Rives Laboratories International, Inc., Wilmington, MA, USA) were provided free access to food and water upon arrival to the vivarium. Rats were housed in individual cages with alternating 12h cycles of light and dark, in temperature and humidity controlled rooms. Ethics approval for animal experimentation was obtained from Washington State University. On day one of the surgical implantation study, the rats were anesthesized using IsoFlo® (isoflurane, USP, Abbott Laboratories, North Chicago, IL, USA) coupled with an oxygen (Oxygen USP, A-L Compressed Gases Inc., Spokane, WA, USA) regulator, and monitored by pedal reflex, and respiration rate to maintain surgical plane of anesthesia. Monoject® 23 gauge (0.6 mm × 25 mm) polypropylene hub hypodermic needles (Sherwood Medical, St. Louis, MO, USA) were used for injection. Undyed braided-coated polyglycolic acid synthetic absorbable surgical suture (Surgical Specialties Corporation, Reading, PA, USA) was used for stitching. Rats were secured to the bench in a dorsal recumbency position with the forelimbs fully extended at 90° angles to the vertebra as to restrict venous return in the jugular vein. Rats were euthanized by overdosing with halothane in bell jar and then administration of a lethal injection of potassium chloride (70%) into the heart. For each of the three density groups (75%, 89.3% and 97.2%) and two time points (6 and 16 weeks), five (n=5) male Sprague Dawley rats (Mean ~300.0 g), hence a total of 15 animals were used in the study.

Following acclimation, all animals underwent a bilateral surgery to create an intramedullary defect in the distal femur (3 mm diameter, 3 mm deep). The defect was created in the lateral condyle by means of a 2-3 mm drill bits. The cavity was rinsed with physiological saline and any bone fragments washed out. The size of the defect was checked using a 3 by 3 mm deep standard cylinder. This defect did not create any lameness and were filled with the titanium implants. On the day of experiment, the animals were implanted with porous Ti6Al4V alloy with three different porosities, 25.0%, 10.7% and 2.8% (control sample). Each animal received a control implant and in addition either 75.0% of 89.3% dense implant in the contralateral leg for each group. One half of the animals from each group were sacrificed 6 weeks post-surgery, while the last group of rats was sacrificed at 16 weeks post-surgery. At necropsy, all the distal femurs were harvested and preserved and implants photographed.

2.2.3 Ion Concentrations in the Implants—Porous Ti6Al4V alloy implants were pushed out of the bone at 6 weeks or were separated from the bone at 16 weeks and weighed. Implants were incubated at 4°C in 2 mL of distilled water and sonicated in an ultrasonicactor for 1 minute. A Shimadzu Atomic Absorption spectrometer AA-6800 (Kyoto, Japan) in the flame ionization mode consisting of an ASC-6100 auto-sampler and hallow cathode calcium lamps were used to determine Ca concentration in the implants as a function of implantation time. Integrations and data collection were carried out using Shimadzu Wizard software (Kyoto, Japan). Stock solutions were freshly prepared in ionization buffer to obtain a final concentration of 2- 4μg/mL. Calcium and ionization buffer standards were purchased from High-Purity Standards (Charleston, SC, USA) and standard curves were prepared at determined concentrations of 0 to 4μg/mL.

2.2.4 Statistics—Five rats were used per treatment groups. The, Ca^{++} concentration in different density groups of implants were compared using a two-way analysis of variance (2ANOVA). When a significant F value was found, *post-hoc* analysis was performed by Bonferroni's multiple comparison tests. In all cases, a P value of < 0.05 was considered significant. Data are presented as mean ± standard error.

3. Results

3.1 Relative Density, Pore Geometry and Microstructures

Typical porous Ti6Al4V samples with different porosities fabricated using LENS™ are shown in Figure 1b. The sample surface clearly showed porosity which was open to the sample surface. The bulk density of laser processed porous Ti6Al4V alloy samples varied from 67 to 85% depending on processing parameters. Influence of various laser parameters on sample density is shown in Table 1. At constant powder feed rate and laser power, increasing scan speed resulted in high porosity in the samples. Similarly, porosity increased with decreasing laser power while other parameters being held constant. Finally, highly porous parts were fabricated by increasing the hatch distance. Figure 2 shows the influence of specific energy input (E) on the bulk density of laser processed Ti6Al4V alloy samples. As expected the bulk density increased with increasing specific energy input. Close observation of this variation indicate the rate of densification is high at low energy input, which gradually decreases at high laser energy inputs. The amount of open pore volume in these LENS™ processed porous samples was evaluated using bulk and apparent densities. The open pore volume fraction varied between 19 to 40% of total porosity. Maximum open pore volume of 40.6% was observed at a scan speed of 25 mm/s and a powder feed rate of 30 g/min.

Evaluation of pore interconnectivity, pore size, and shape was done by performing microstructural study on both part build direction and perpendicular to part build direction of porous Ti6Al4V structures. The build direction refers to the z-axis or part axis. Although bulk

density decreased with increase in the scan speed or powder feed rate or decrease in the laser power, no significant change in the pore diameter was observed. However, hatch distance was found to have strong influence on pore diameter and the mean pore diameter increased with an increase in the hatch distance. The mean pore diameter of the samples made with 0.762 mm hatch distance was in the range 60 - 700 ± 20 μm and hatch distance of 1.27 mm resulted in mean pore diameter between 300 and 1500 ± 90 μm. Figure 3 shows that the pore interconnectivity was different in different directions. In general, there was more connectivity between the pores along the build direction than in perpendicular to build direction as shown in Figures 3a and b. However, the pore connectivity was relatively more uniform in both directions when the density was decreased below ~75% as shown in Figures 3c and d.

Typical matrix microstructures of as-received Ti6Al4V alloy powder and laser processed porous samples are shown in Figure 4. As-received powder and laser processed samples showed a mixture of α and β phases in the microstructures. However, it was found that the laser processing increases the needle shaped β phase. These observations were confirmed by XRD study on as-received powder and laser processed Ti6Al4V alloy samples as shown in Figure 5. The results show that a considerable amount of high temperature β phase is retained at room temperature in laser processed samples. In addition, relatively higher amount of β phase in laser processed samples along with finer α phase resulted in higher average hardness of 347 ± 18 HV when compared to the hardness of 308 ± 28 HV for as-received alloy powder. Table 1 shows Vicker's microhardness measurements of LENS™ processed porous Ti6Al4V alloy samples fabricated under various processing conditions. Since the microstructure of these samples did not change significantly due to various laser parameters used in the present work, the hardness of various samples was also within the standard deviation of average hardness of 347 ± 18 HV.

3.2 Mechanical Properties

Mechanical properties of laser processed porous Ti6Al4V alloy structures are shown in Figures 6 and 7. The data indicates that the Young's modulus of the laser processed porous samples can be varied between 7 to 60 GPa by changing the LENS™ process parameters. The modulus of laser processed samples having porosity in the range of 23 to 32 vol% is close to that of the human cortical bone. The average 0.2% proof strength of LENS™ processed porous Ti6Al4V alloy structures was between 471 to 809 MPa.

3.3 In vivo Behavior of Laser Processed Porous Ti6Al4V alloy Implants

The results indicate that the rats initially lose up to 20% of their initial body weight after surgery and start to regain weight after the first week of surgery. Rats sacrificed after 6 weeks of surgery required some force to push out the implant from the bone indicating initial biological fixation between the porous implant and the living tissue. However, at 16 weeks, it was impossible to push out the 75% dense implant from the bone due to strong bonding with the bone as result of biological tissue ingrowth. Moreover, the bonding was significantly high for implants with highest porosity, i.e., 25% porosity.

To corroborate the weight change observations, porous Ti alloy implants were characterized in terms of their calcium content at 6 and 16 weeks after surgery. The results, shown in Figure 8, indicate that significant increase in Ca^{++} concentration was apparent in implants with 25% porosity only after 6 weeks. Other implants with 10.7% and 2.8% porosity showed very low Ca^{++} concentration content. Changes in calcium content within the implants showed an increase at both 6 weeks and 16 week time points in which an increase in concentration was dependent on porosity. Figure 9 demonstrates typical tissue ingrowth in the present laser processed titanium alloy implants at 16 weeks post-implantation. Significant biological tissue

ingrowth is apparent in the 75% porosity Ti6Al4V implants compared to the implants with two other porosities.

4. Discussion

Current experimental results demonstrate that the properties of porous metallic biomaterials can be tailored to suit human bone properties, by using different design approaches in combination with appropriate laser processing parameters. It is also shown that the amount of porosity that can be introduced in the LENS™ processed samples is directly related to the specific laser energy input, consequently the extent of powder melting, depending on the process parameters. At constant laser power and powder feed rate, high scan speeds decreases the specific energy input by decreasing the interaction time between the powders and the laser. Lower energy input means lower working temperatures and hence low amount of liquid phase around the powder particles due to partial melting of the powder. These surface melted powders join together in the presence of liquid metal at the particle interfaces, leaving some interparticle residual porosity. Particle bonding during LENS™ processing is the result of localized melting and subsequent solidification as against solid state sintering in powder metallurgical route. Therefore, the inherent brittleness associated with solid state sintered metal powders is completely eliminated in laser processed porous samples. Moreover, intensifying the specific energy input by increasing the laser power increases the working temperatures and consequently melts the powder completely leading to dense deposit/layer. In addition, at high working temperatures the flow of liquid metal to fill the inter particle pores becomes easier and promotes higher densification than at low working temperatures. Higher porosity at large hatch distance is due to the fact that powders will be deposited at wider spacing between successive scans. Although, total porosity is important in reducing the effective modulus of porous metals, the amount of open pore volume is very important for biomedical applications. High amount of open pores in the samples will allow more body fluids to be transported to the interior of the implant through the interconnected pores, which will subsequently accelerate the healing process allowing tissue to grow inside the implants. The open pore volume varied between 19 to 40% of total porosity for our samples. Although there is no clear trend, the laser parameters which increased the total pore volume also increased the open pore volume.

The increase of pore size and interconnectivity due to the increase of hatch distance is caused by the reduction of the overlap region between the successive scans and the increase in the space between successive laser scans. At low hatch distance, due to high amount of re-melting of existing solidified road by the next scans results in higher densification in this region. The discrepancy in pore connectivity in different directions is attributed to the selection of distance between two successive scans in each layer, thickness of each metal layer and the deposition angles of laser scans for each layer. Since the scan distance and thickness of each layer is constant, the pores are regularly arranged along the build direction. In this case, the pore connectivity in the perpendicular to build direction is predominantly influenced by the other processing parameters such as laser power, scan speed and powder feed rate, which can change the porosity within the metal lines and hence their connectivity. Therefore, better connectivity between pores is ensured in low density samples by changing those parameters. In the case of high density samples, the pores can be oriented layer by layer via changing the deposition angles in each layer leading to a three-dimensionally interconnected porosity.

The retention of high temperature β phase in the laser processed samples is attributed to the high cooling rates associated with laser processing which do not allow sufficient time for the high temperature β phase to transform to low temperature α phase. It is important to note that presence of β phase can not degrade the biocompatibility of these samples, as both α + β Ti and β Ti alloys are widely used for biomedical applications. High hardness of laser processed material is attributed to high solidification rates of laser processing, which leads to the

formation of finer α phase and retention of more high temperature β phase at room temperature. Similar microstructures of various laser processed structures indicate that process is reproducible. It has been shown that the microstructure of laser processed porous samples had no influence on their biocompatibility [6]. Only pore characteristics such as pore size and shape found to have strong influence on cell-materials interactions [6]. Therefore, microstructural variations such as high amount of β phase in the laser processed Ti6Al4V alloy samples can not degrade their biocompatibility.

The density range difference between the porous Ti6Al4V samples and that of natural bone is due to the inherent high density of Ti6Al4V alloy. Although the density is high, it is imperative to notice that modulus matched to that of natural bone. The elastic modulus varied depending on porosity of the structures. It was observed that the higher the porosity the lower the modulus, which is attributed to the introduction of porosity in the samples. Estimated modulus values using Equation 2 (Nielsen's relationship [34]) are compared with experimental values in Figure 7. The discrepancies between calculated and experimental modulus values, especially at low densities, are presumably due to the influence of pore geometry, neck size, stress concentrations and microstructural variations. However, at higher densities good agreement was observed between experimental and theoretically estimated values. It is important to note from the Nielsen's relation that the shape or geometry factor of the pores can strongly influence the modulus of porous samples. This relation indicates that by changing the pore geometry from more regular (spherical pore with geometry factor of 1) to irregular shape the modulus of porous metals can be decreased. For example, one can make implants with identical porosities but with different moduli. Therefore, LENS™ provides more flexibility for designers to tailor the modulus of these porous implants without changing their bulk density or total pore volume, which is impossible via conventional processing routes such as powder sintering. This is because it is possible to tailor the pore shape in LENS™ processed porous implants by changing distance between two successive laser scans in each successive layers during fabrication. The moduli of as-processed porous Ti6Al4V between 7 and 60 GPa cover the modulus of human cortical bone which has a modulus in the range of 3 to 20 GPa.

The *in vivo* biocompatibility results with male Sprague-Dawley rats in a 16 week study show that the laser processed samples promote tissue ingrowth through the interconnected porosity. Apart from the porosity, the rough surface morphology within the pores also helps in biological tissue attachment and growth in these laser processed samples [6,36-38]. Three sets of samples were used with total porosity of 25%, 10.7 % and 2.8% volume porosity. The *in vivo* results clearly showed the influence of the amount of porosity on biological tissue integration. A high amount of open pore volume allowed more body fluids to be transported through the interconnected pores, which subsequently accelerated the healing process by allowing tissue to grow inside the implants and improved the biological fixation. High amount of Ca^{++} concentration in 25% porosity samples demonstrated this. For samples with low volume fraction porosity, significantly less Ca^{++} concentration was noticed due to less amount of body fluids transported through the available open pore volume. These results suggest that there could be a critical amount of porosity needed in these implants to initiate formation of the biological tissue. Considerable amount of ion concentration suggests the formation of new tissue in the pores of these porous Ti6Al4V alloy implants. In addition, there appeared to be a peak in the calcium concentrations at 6 weeks, which decreases at 16 weeks. Though the exact reason for this variation is not clear, this may suggest remodelling or tissue matrix being replaced by other factors at these early time points. Furthermore, the effects of stress shielding inside the porous implants may occur. Similar bone remodeling process up to 12 weeks in porous CoCrMo alloy implants has been reported [39], where both the mature and less mature bone were found in the pores.

Overall, *in vivo* results show that the pore interconnectivity is very important for the implants to show positive influence on osteoconductive properties of metallic implants. These results also demonstrate that the laser processing do not change the inherent *in vivo* biocompatibility of metallic biomaterials. Our results suggest that LENS™ process enables us to fabricate net shape implants with designed porosities, which can be extended to other metallic biomaterials without altering their purity and biological properties.

5. Conclusions

LENS™ can be used to fabricate net shaped, functional implants to meet individual patient needs and can be extended to other metallic biomaterials as well. Under the present experimental conditions, the total porosity of Ti6Al4V samples varied in the range of 18 to 32%. Depending on the porosity, the elastic modulus varied between 7 and 60 GPa and 0.2% proof strength between 471 and 809 MPa. Porous Ti6Al4V alloy structures with 23 to 32 vol % porosity have modulus equivalent to natural bone. Open pore volume faction up to 0.40 of total porosity in these samples can accelerate the healing process through biological fixation. This has been demonstrated *in vivo* with male Sprague-Dawley rats in a 16 week study with samples having 25%, ~11% and ~3% total porosity. After 16 weeks, the 25% porosity samples showed the highest amount of Ca^{++} concentration within the pores suggesting a faster rate of tissue generation and integration compared to samples with lower pore volume.

Acknowledgments

Authors would like to acknowledge the Office of Naval Research (Grant No. N00014-1-04-0644 and N00014-1-05-0583), the National Science Foundation (Grant No. CMMI 0728348) and the National Institutes of Health (Grant No. NIH-R01-EB-007351) for the financial support. Financial support from the W. M. Keck Foundation to establish a Biomedical Materials Research Lab at WSU is also acknowledged.

References

1. Robertson DM, Pierre L, Chahal R. Preliminary observations of bone ingrowth into porous materials. J Biomed Mater Res 1976;10:335–344. [PubMed: 1270453]
2. Cameron HU, Macnab I, Pilliar RM. A porous metal system for joint replacement surgery. Int J Artif Organs 1978;1:104–109. [PubMed: 680998]
3. Head WC, Bauk DJ, Emerson RH Jr. Titanium as the material of choice for cementless femoral components in total hip arthroplasty. Clin Orthop Relat Res 1995;311:85–90. [PubMed: 7634595]
4. Ryan, Garrett; Pandit, Abhay; Apatsidis, Dimitrios Panagiotis. Fabrication methods of porous metals for use in orthopaedic applications. Biomaterials 2006;27:2651–2670. [PubMed: 16423390]
5. Krishna, B Vamsi; Bose, Susmita; Bandyopadhyay, Amit. Low stiffness porous Ti structures for load-bearing implants. Acta Biomater 2007;3:997–1006. [PubMed: 17532277]
6. Weichang, Xue; Krishna, B Vamsi; Bandyopadhyay, A.; Bose, S. Processing and biocompatibility evaluation of laser processed porous titanium. Acta Biomater 2007;3:1007–1018. [PubMed: 17627910]
7. Jia Ping L, Pamela H, Mirella D, Clayton EW, Joost RW, Clemens AB, Klaas G. Bone ingrowth in porous titanium implants produced by 3D fiber deposition. Biomaterials 2007;28:2810–2820. [PubMed: 17367852]
8. Bungo O, Mitsuru T, Shunsuke F, Masashi N, Tadashi K, Takashi N. Pore throat size and connectivity determine bone and tissue ingrowth into porous implants: Three-dimensional micro-CT based structural analyses of porous bioactive titanium implants. Biomaterials 2006;27:5892–5900. [PubMed: 16945409]
9. Kenzo A, Norihiko K, Osamu O, Ishi M. Mechanical properties and biomechanical compatibility of porous titanium for dental implants. J Biomedical Materials Research 1985;19:699–713.
10. Oh IH, Nomura N, Masahashi N, Hanada S. Mechanical properties of porous titanium compacts prepared by powder sintering. Scripta Mater 2003;49:1197–1202.

11. Pillar RM. P/M Processing of Surgical Implants: Sintered Porous Surfaces for Tissue-to-Implant Fixation. Int J Powder Metallurgy 1998;34(8):33–46.
12. Wen CE, Mabuchi M, Yamada Y, Shimojima K, Chino Y, Asahina T. Processing of biocompatible porous Ti and Mg. Scripta Mater 2001;45:1147–1153.
13. Pillar RM. Porous-surfaced metallic implants for orthopaedic applications. J Biomed Mater Res – Appl Biomater 1987;21(A1):1–33.
14. Young FA, Spector M, Kresch CH. Porous titanium endosseous dental implants in rhesus monkey: microradiography and histological evaluation. J Biomed Mater Res 1979;13:843–856. [PubMed: 117007]
15. Hahn H, Palich W. Preliminary evaluation of porous metal surface titanium for orthopedic implants. J Biomed Mater Res 1970;4:571–577. [PubMed: 5487557]
16. Park, JB.; Lakes, RS. Biomaterials: an introduction. 2nd. Plenum; New York: 1992.
17. Walt MJ, Lamprecht EG. Bone ingrowth into an open porous surface. Trans Orthop Res Soc 1992;38:360–365.
18. Jasty M, Bragdon CR, Haire T, Mulroy RD, Harris H. Comparison of bone ingrowth into cobalt chrome sphere and titanium fiber mesh porous coated cementless canine acetabular components. J Biomed Mater Res 1993;27:639–644. [PubMed: 8314816]
19. Fujisawa A, Noda I, Nishio Y, Okimatsu H. The development of the new titanium arc-sprayed artificial joints. Mater Sci Eng C 1995;2:151–157.
20. Bloebaum RD, Mihalopolulus NL, Jensen JW, Dorr LD. Post mortem analysis of bone growth into porous-coated acetabular components. J Bone Joint Surg 1997;79:1013–1022. [PubMed: 9234877]
21. Stephen DC, Frederick G, Harry BS, Ray JH. Fatigue properties of carbon and porous coated Ti6Al4V alloy. J Biomed Mater Res 1984;18:497–512. [PubMed: 6736080]
22. Yue S, Pilliar RM, Weatherly GC. The fatigue of porous coated Ti6Al4V implant alloy. J Biomed Mater Res 1984;18:1043–1058. [PubMed: 6544792]
23. Staiger MP, Pietak AM, Huadmai J, Dias G. Magnesium and its alloys as orthopedic biomaterials: A review. Biomaterials 2006;27:1728–1734. [PubMed: 16246414]
24. Vassilis K, David K. Porosity of 3D biomaterial scaffolds and osteogenesis. Biomaterials 2005;26:5474–5491. [PubMed: 15860204]
25. Kalpana SK. Biomaterials in total joint replacement. Colloids and Surfaces B: Biointerfaces 2004;39:133–142.
26. Mitsuo N. Recent metallic materials for biomedical applications. Met and Mater Trans 2002;33A: 477–486.
27. Mullen, Lewis; Stamp, Robin C.; Brooks, Wesley K.; Jones, Eric; Sutcliffe, Christopher J. Selective laser melting: A regular unit cell approach for the manufacture of porous, titanium, bone ingrowth constructs, suitable for orthopedic applications. J Biomed Mater Res Part B: Appl Biomater 2008;89B:325–334. [PubMed: 18837456]
28. Traini T, Mangano C, Sammons RL, Mangano F, Macchi A, Piattelli A. Direct laser metal sintering as a new approach to fabrication of an isoelastic functionally graded material for manufacture of porous titanium dental implants. Dental materials 2008;24:1525–1533. [PubMed: 18502498]
29. Wu X, Mei J. Near net shape manufacturing of components using direct laser fabrication technology. J Matl Proc Technol 2003;135:266–270.
30. Gary KL, Eric S. Practical considerations and capabilities for laser assisted direct metal deposition. Materials and Design 2000;21:417–423.
31. Krishna, B Vamsi; Bose, Susmita; Bandyopadhyay, Amit. Fabrication of Porous NiTi Shape Memory Alloy Samples using Laser Engineered Net Shaping. J Biomed Mater Res Part B – Appl Biomater 2009;89B:481–490. [PubMed: 18937263]
32. Krishna, B Vamsi; Xue, Weichang; Bose, Susmita; Bandyopadhyay, Amit. Engineered Porous Metals for Implants. JOM 2008;60(5):45–48.
33. Simchi A, Pohl H. Effects of laser sintering processing parameters on the microstructure and densification of iron powder. Mater Sci and Eng A 2003;359:119–128.
34. Nielsen LF. Elasticity and damping of porous materials and impregnated materials. J Am Ceram Soc 1984;67(2):93–98.

35. Quintana, LluÍs; zur Nieden, Nicole I.; Semino, Carlos E. Morphogenetic and regulatory mechanisms during developmental chondrogenesis: new paradigms for cartilage tissue engineering. Tissue Engineering: Part B 2009;15(1):29–41.

36. Das K, Krishna B Vamsi, Bose S, Bandyopadhyay A. Surface Modification of Laser Processed Porous Titanium for Load Bearing Implants. Scripta Materialia 2008;59:822–825.

37. Das K, Bose S, Bandyopadhyay A. Surface Modifications and Cell-Materials Interactions with Anodized Ti. Acta Biomaterialia 2007;3:573–585. [PubMed: 17320494]

38. Roy M, Krishna BV, Bandyopadhyay A, Bose S. Laser processing of bioactive tricalcium phosphate coating on titanium for load-bearing implants. Acta Biomaterialia 2008;4(2):324–333. [PubMed: 18039597]

39. Cook SD, Walsh KA, Haddad RJ Jr. Interface Mechanics and Bone Growth into Porous Co-Cr-Mo Alloy Implants. Clin Ortho Relat Res 1985;193:271–280.

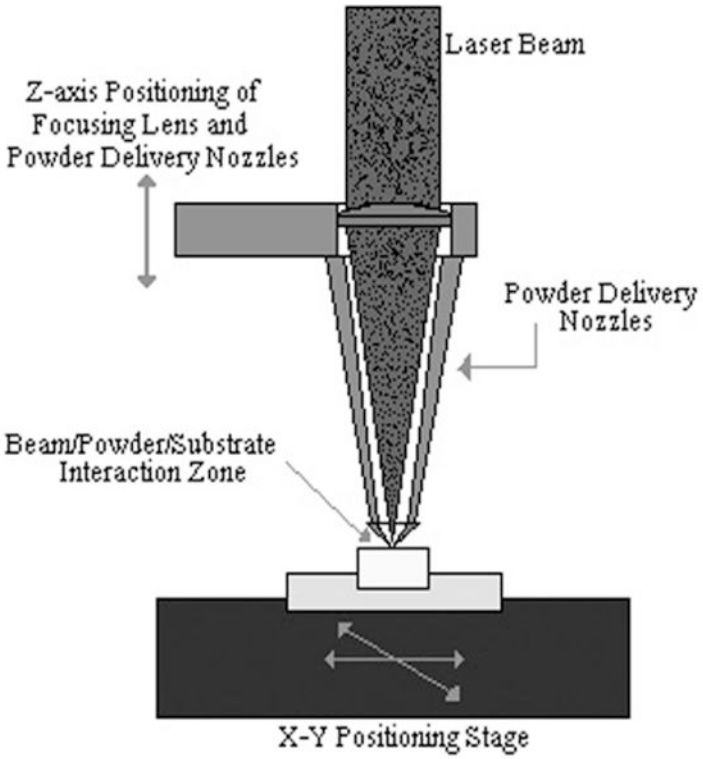

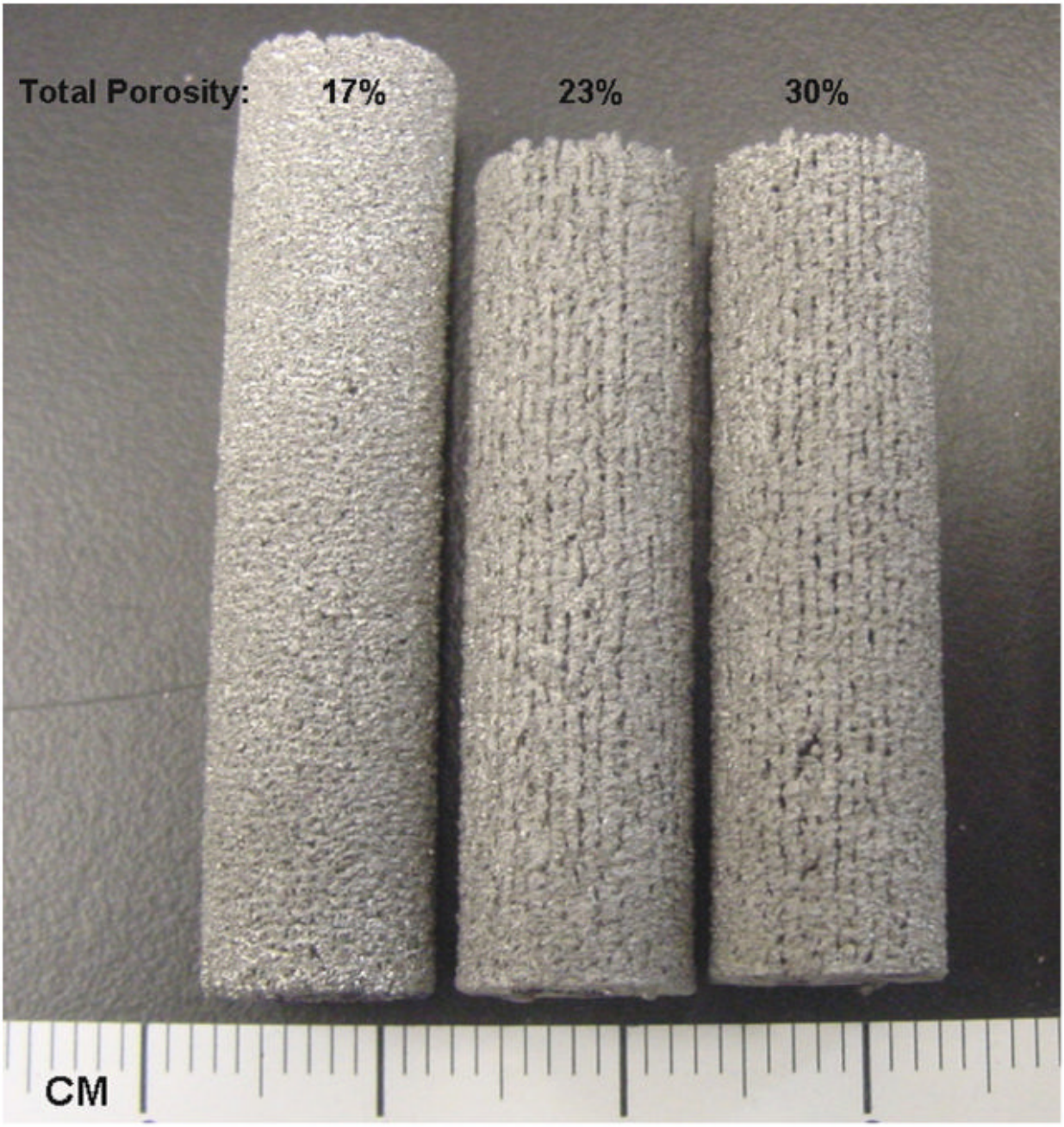

Fig. 1.
(a) Schematic depiction of LENS™ process (b) typical porous Ti6Al4V samples fabricated using LENS™.

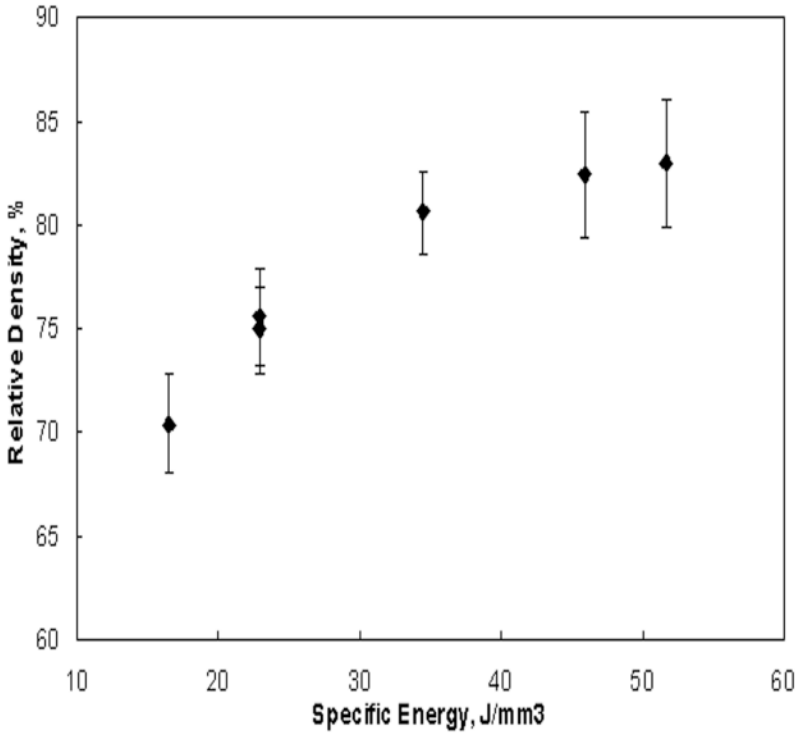

Fig. 2.
Influence of specific energy input on the relative density of laser processed Ti6Al4V alloy samples.

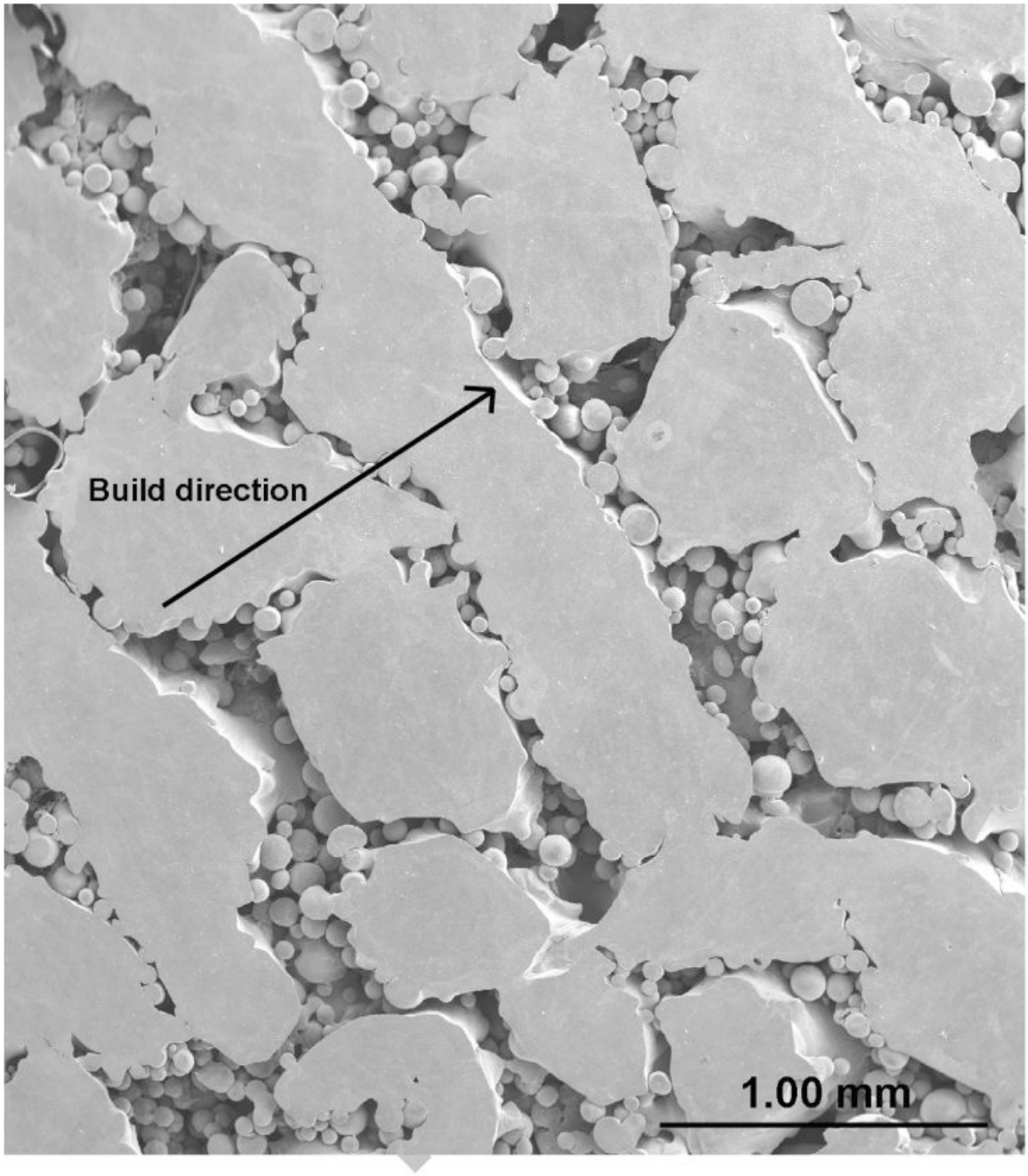

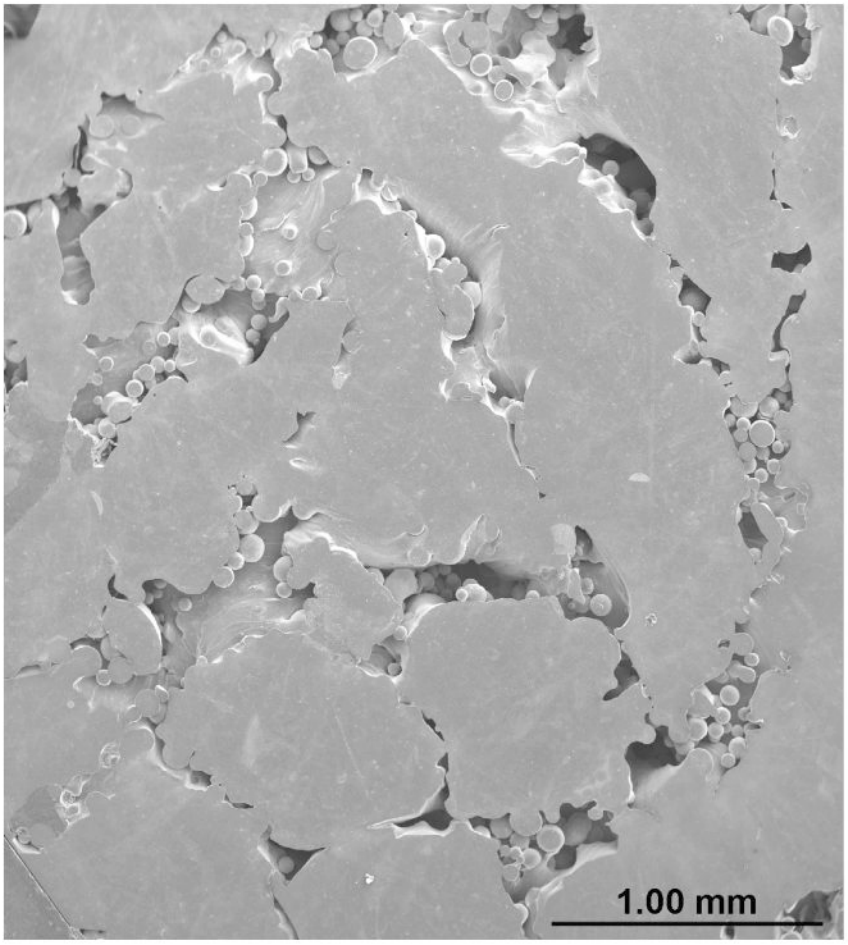

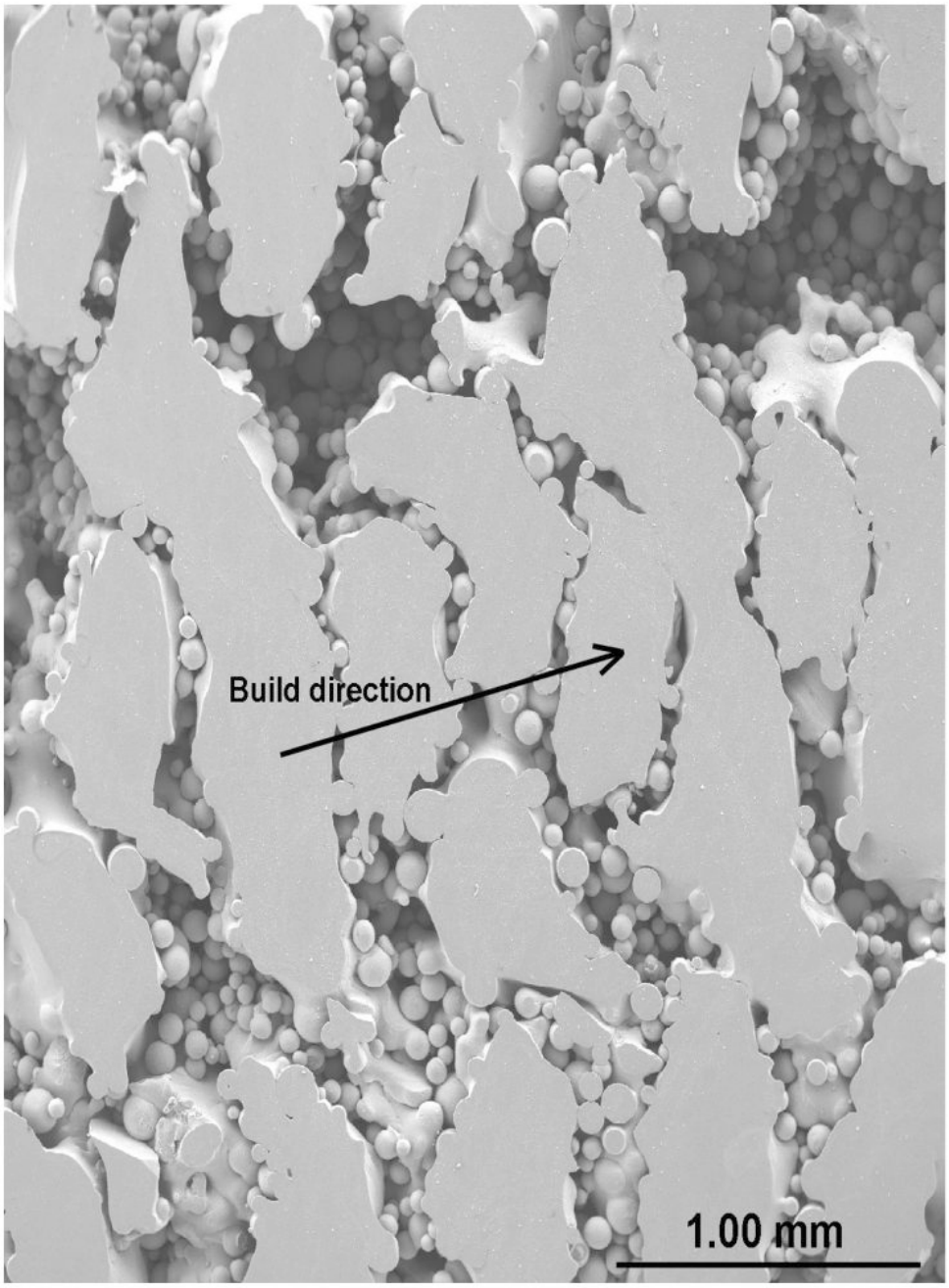

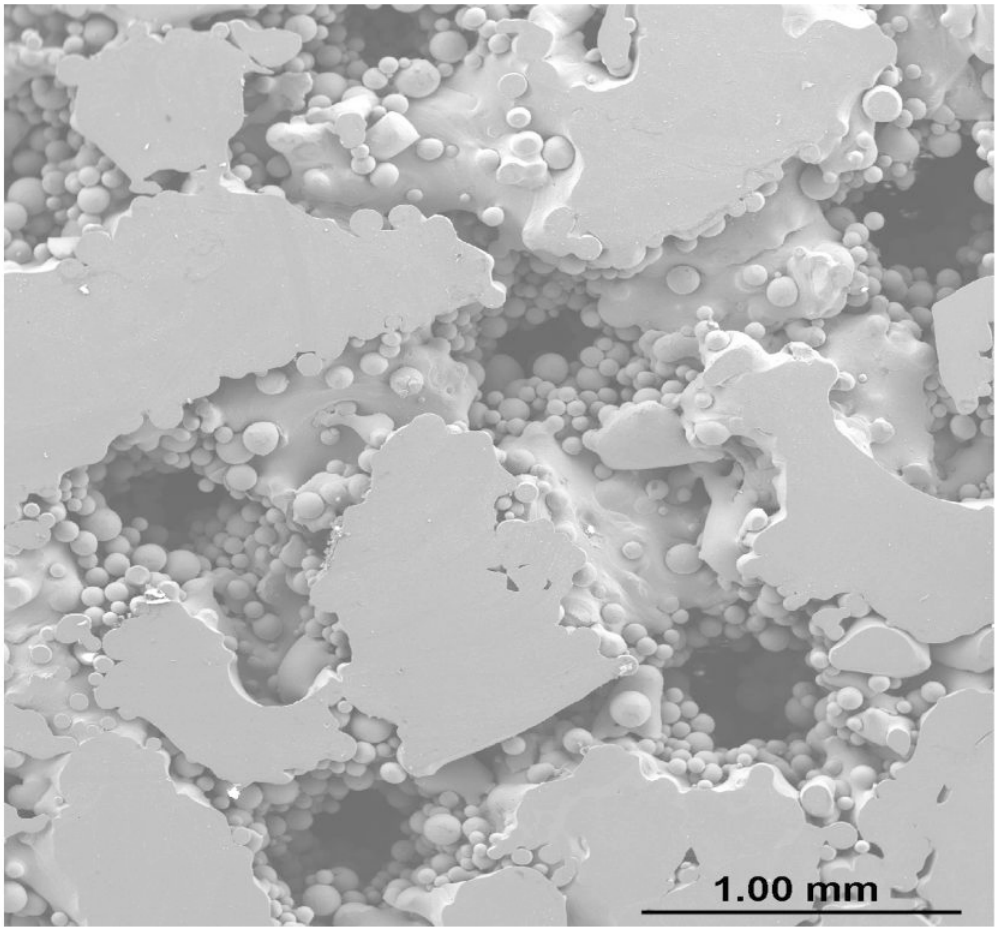

Fig. 3.
Micrographs showing pore connectivity (a) Part build section, 180W, 15g/min, 10 mm/s, 0.762mm, relative density 80% (b) Same as (a) Perpendicular section, (c) Part build section, 200 W, 30g/min, 25mm/s, 1.27mm, relative density 70% (d) Same as (c) Perpendicular section.

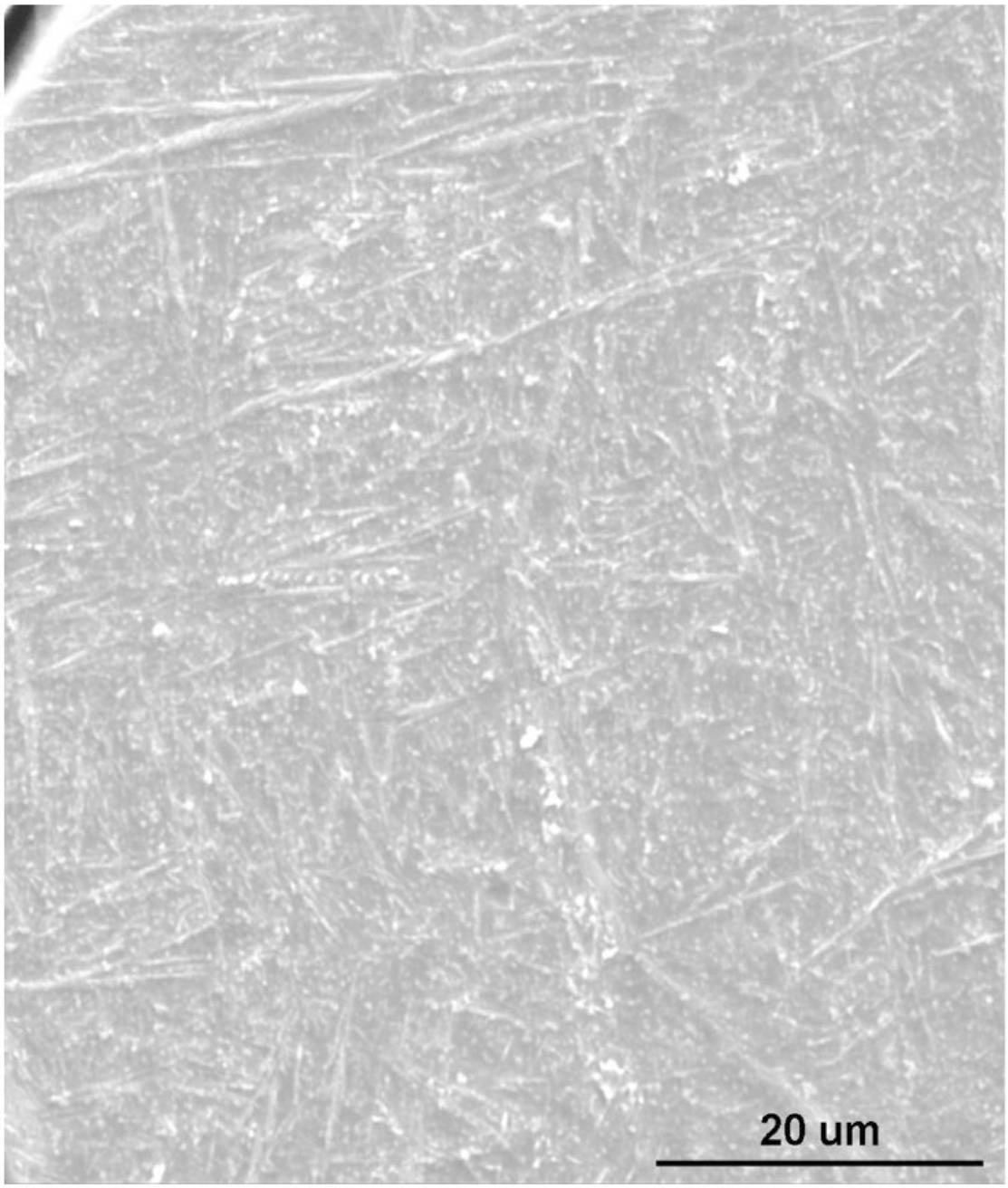

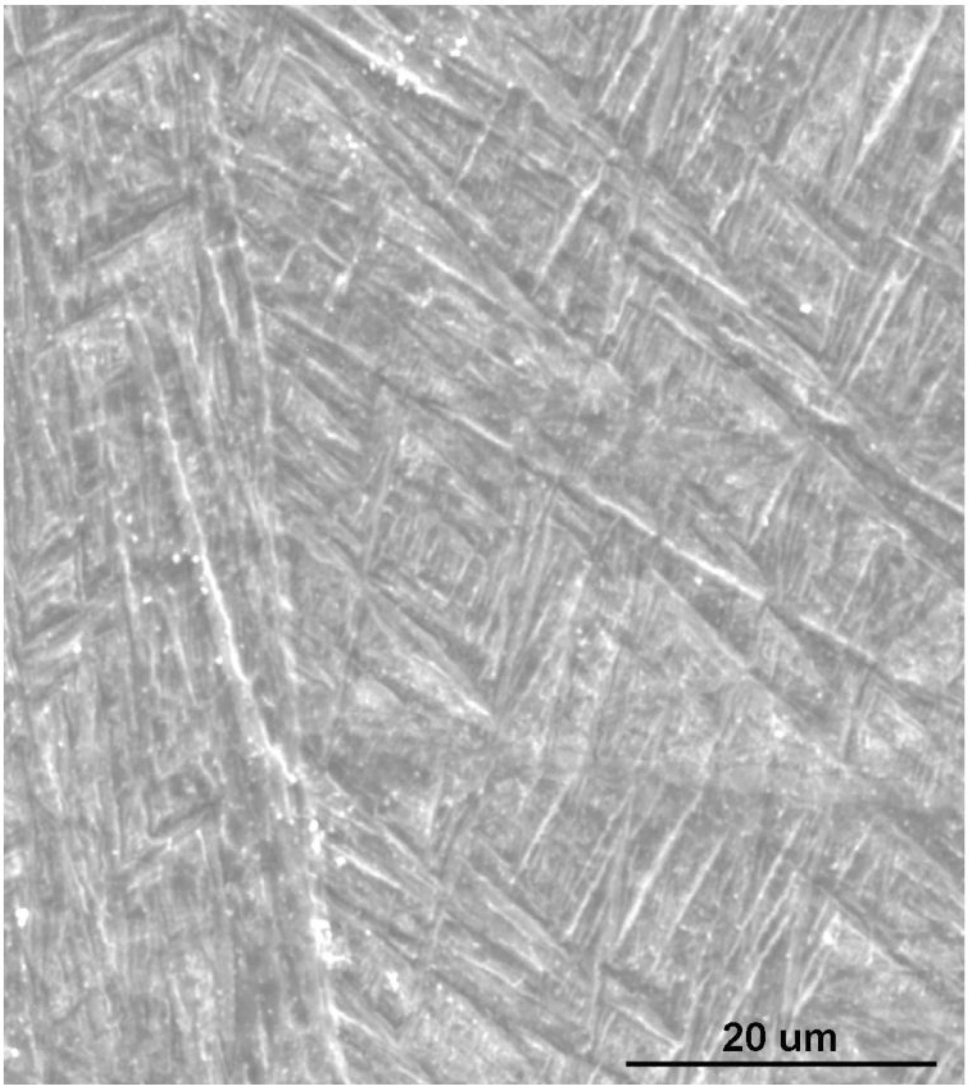

Fig. 4.
Typical microstructure of (a) as-received powder (b) laser processed samples.

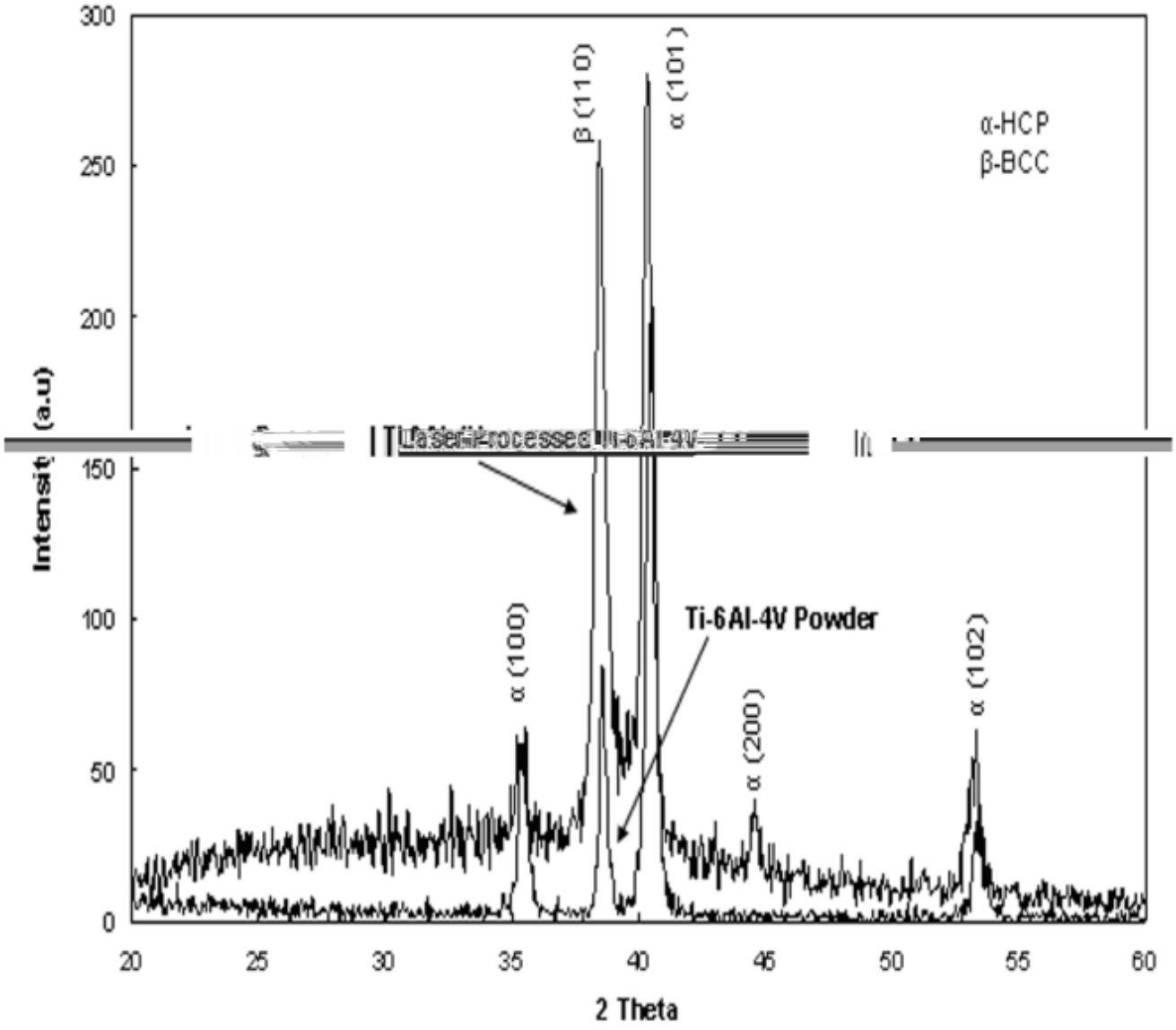

Fig. 5.
X-ray diffraction pattern of laser processed structures and as-received Ti6Al4V alloy powder.

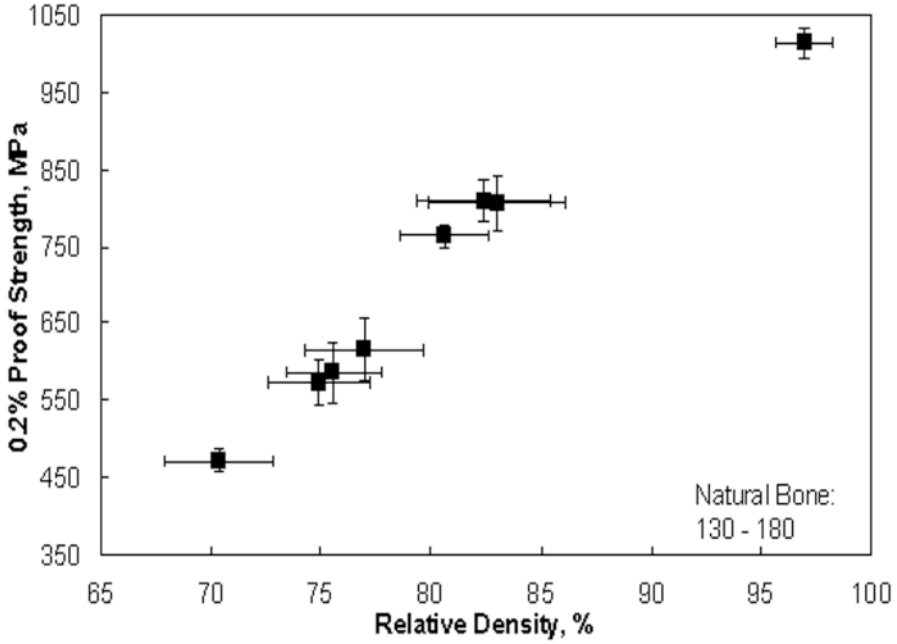

Fig. 6.
0.2% proof strength of laser processed porous Ti6Al4V samples.

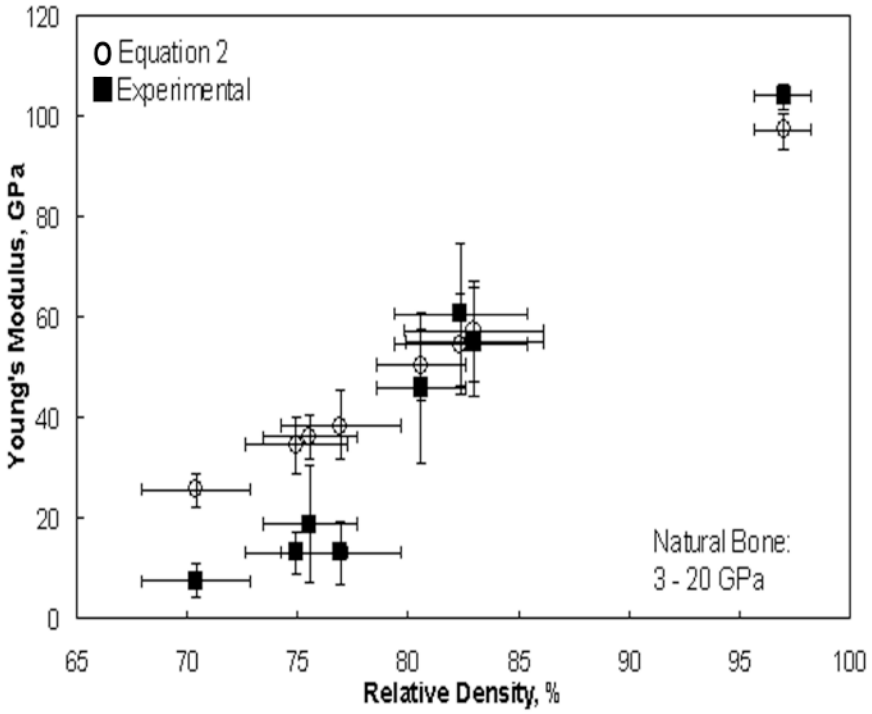

Fig. 7.
Young's modulus of laser processed porous Ti6Al4V samples.

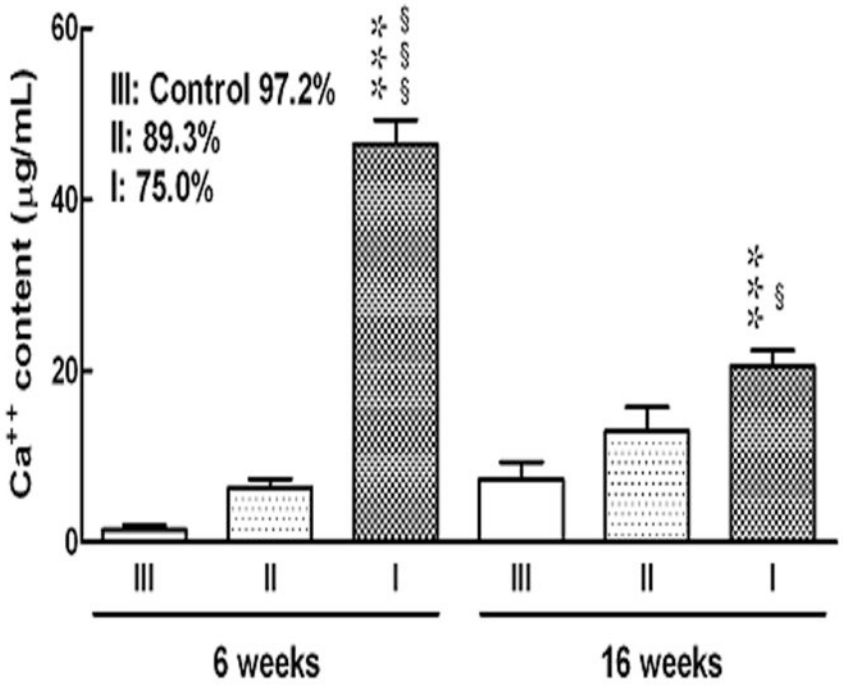

Fig. 8.

Ca^{++} concentration in porous Ti6Al4V alloy implants. Each bar indicates the mean concentration of Ca^{++} and each vertical line indicated the S.E.M. of 5 rats per group. *** P<0.001 vs. III, §§§ P<0.001 vs. II

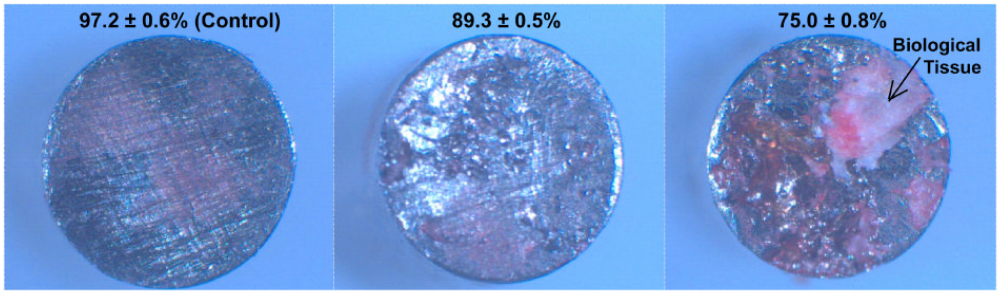

Fig. 9.
LENS processed porous Ti6Al4V implants after 16 weeks implantation in rat intramedullary defects.

Table 1

Hardness, bulk density and laser processing parameters used to fabricate porous Ti6Al4V structures.

Sample	Laser Parameters				Specific Energy, J/mm^3	Relative Density, %	Open pore vol. fraction	Hardness
	Laser Power, W	Scan Speed, mm/s	Feed rate, g/min	Hatch Distance, mm				
1	180	10	15	0.762	46.5	76.94 ± 2.6	0.34	331 ± 12
2	200	10	15	0.762	51.7	82.98 ± 3.0	0.19	339 ± 18
3	200	15	20	0.762	34.4	80.59 ± 2.0	0.26	357 ± 10
4	200	15	35	0.762	45.9	82.40 ± 3.0	0.25	350 ± 12
6	200	18	35	1.27	22.9	74.91 ± 2.3	0.37	353 ± 22
5	200	18	30	1.27	22.9	75.55 ± 2.1	0.33	351 ± 21
7	200	25	30	1.27	16.5	70.39 ± 2.4	0.40	343 ± 21

Table 2

LENS™ parameters for in vivo porous Ti6Al4V alloy samples.

Sample	Laser Parameters			Relative Density, %	Open pore vol. fraction
	Laser Power, W	Scan Speed, mm/s	Feed rate, g/min		
I	100	18	38.5	75.0 ± 3.4	0.4
II	200	18	36.8	89.3 ± 3.8	0.07
III (control)	350	18	15.6	97.2 ± 1.3	0